Biomacromolecules

pubs.acs.org/Biomac

Article

Supramolecular Assembly of β-Cyclodextrin-Modified Polymer by Electrospinning with Sustained Antibacterial Activity

Wenshi Xu, Yong Chen, Bing Zhang, Wenwen Xu, Jie Niu, and Yu Liu*

Cite This: https://doi.org/10.1021/acs.biomac.1c01007

Read Online

ACCESS | Metrics & More | Article Recommendations | Supporting Information

ABSTRACT: Supramolecular assembly loading drug as biomedical materials is a research hotspot. Herein, we reported a supramolecular electrospun assembly constructed via the hydrophobic and hydrogen bonding interaction. The obtained results showed that the assembly by supramolecular electrospinning not only increased the interactions of multiple antibacterial active species including antibiotics, cationic polymers, and silver to form a flexible membrane with good mechanical strength but also indicated the dual effects of rapid doxycycline and polyethyleneimine release as well as a sustained Ag release. Interestingly, the assembly showed not only good degradability but also a high bacteriostatic efficacy toward *Escherichia coli* (*E. coli*) up to 99.9%. More importantly, the in vivo wound healing assay indicated that the assembly could promote the healing of uninfected, *E. coli*-infected, and even methicillin-resistant *staphylococcus aureus*-infected wounds. The current research provides a novel approach to construct a supramolecular assembly by electrospinning mechanically induced strong noncovalent interaction.

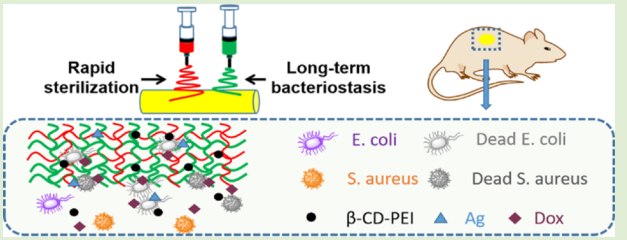

INTRODUCTION

Due to the widespread use of antibiotics, the number of antibiotic-resistant pathogens has increased significantly, posing a great threat to human health.[1−5] It will take a long time and high cost to develop new antibiotics for clinical use.[6] Therefore, researchers in related fields are trying to explore new ways to solve the problems caused by antibiotic resistance.[7,8] Supramolecular chemistry, one of the most popular chemical subfields, is a highly interdisciplinary research discipline[9] and can be used in various fields.[10−15] Because noncovalent interaction has the characteristics of flexibility and adjustment,[16] a supramolecular system can incorporate a variety of functional active agents according to different requirements.[17] Therefore, supramolecular antibacterial materials have great advantages and broad application prospects.[18−20] Antibiotics, cationic polymers, metals, etc., are usually used as antibacterial materials.[21−23]

Jin et al. reported several *N*-diazeniumdiolate-functionalized β-cyclodextrin (β-CD) derivatives which had great bactericidal activity against *pseudomonas aeruginosa* via releasing nitric oxide and co-delivering a hydrophobic drug.[24] Machelart et al. demonstrated that the nanoparticles made from cross-linked poly-β-cyclodextrin (pβCD) could be used as effective drug carriers and had inherent antibacterial properties.[25] Suárez investigated the structure and thermodynamic parameters of free Dox and the Dox/β-CD complex, and found that Dox/β-CD had more effective antibacterial activity.[26] These researches indicated that the combination of β-CD and antibiotics can increase their antibacterial effect.

It is well known that some cationic polymers interact with negatively charged bacterial cells, destroying the integrity of their cell membranes and leading to the death of bacteria.[1] A series of quaternized β-chitin derivatives were recently reported with excellent antimicrobial activities against *Escherichia coli*, *Staphylococcus aureus*, *Candida albicans*, and *Rhizopus oryzae*, which can be used as dressings for clinical skin regeneration.[27] PEI comprised of primary, secondary, and tertiary amino groups can be protonated in an acidic environment and is positively charged. Moreover, PEI can form hydrogen bonds and coordination bonds with other substances containing $-NH_2$, $-OH$, $-F$, $-C{=}O$ or a coordinated central atom. We constructed a supramolecular nanoparticle by sulfato-β-cyclodextrin (SCD) and PEI via electrostatic interactions for loading and sustaining the release of ATP.[28] Li et al. reported soy protein isolate (SPI)/PEI-Cu and SPI/PEI-Zn films and demonstrated that they have high bacterial resistance against *E. coli* and *Staphylococcus aureus* (*S. aureus*).[29]

Silver affects bacterial membranes, enzymes, and nucleic acid activities through coordination, owning good bactericidal and antibacterial effects.[30,31] We constructed a supramolecular hydrogel from biocompatible building blocks chitosan, β-CD, and Ag^+, exhibiting high wound healing ability and excellent antibacterial effect.[17] Shi et al. reported an Ag-self-pumping

Received: August 4, 2021

Scheme 1. Schematic Diagram of the PVA/Dox@β-CD-PEI/PCL/Ag Nanofibrous Membrane Prepared by Electrospinning Technology and Its Bactericidal and Bacteriostatic Properties as Wound Dressing; Red Fibers Represent PVA/Dox@β-CD-PEI, Green Fibers Represent PCL/Ag

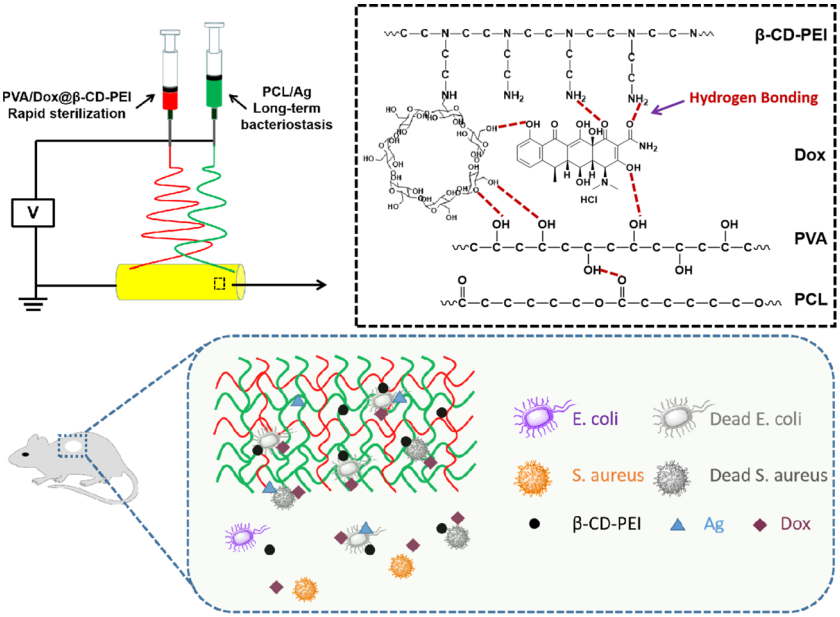

dressing doped with Ag nanoparticles, accelerating the wound healing process.[32] Lv et al. reported the synthesis of silicon nanowires (SiNWs) with in situ-grown silver nanoparticles and demonstrated the highly effective and long-term antibacterial activity of this novel nanostructure.[33]

However, all kinds of active antibacterial agents have their advantages and disadvantages.[18] The combination of different antibacterial agents is used to balance these characteristics and play a synergistic effect of complementing each other. In addition, research on sustained antibacterial materials that reduce the repeated use of antibiotics is of great significance.[34] Moreover, porous nanofibrous membrane prepared by electrospinning has the advantages of adjustable porosity, good ductility, good air permeability, and light weight. As a wound dressing, it not only has a physical shielding effect but also inhibits bacterial infection, promotes cell proliferation, and accelerates wound healing. Herein, we proposed a new supramolecular electrospun assembly bifunctional antibacterial membrane, which was composed of a persistent antibacterial polycaprolactone/Ag (PCL/Ag) substrate membrane and a hydrolysable fast bactericidal polyvinyl alcohol (PVA)/Dox@β-CD-PEI membrane. The preparation process is shown in Scheme 1. One of the advantages of this system is that the supramolecular electrospun assembly antibacterial membrane could release antibacterial active substance Dox and PEI rapidly and release Ag slowly for a long time, which provided rapid sterilization and long-lasting antibacterial effect. When used as wound dressing, it can kill bacteria at the wound quickly, and release silver slowly to inhibit the growth of bacteria, avoiding the pain caused by frequent dressing replacement and promoting wound healing. In addition, another advantage of this work is the synergistic effect of a variety of antibacterial active substances, so as to avoid the bacterial resistance caused by high antibiotics usage and the potential cytotoxic harm caused by high silver content. Therefore, it has great potential to be used in wound dressing applications.

EXPERIMENTAL SECTION

Materials. PVA1750 ± 50 was purchased from Heowns Biochem LLC. Doxycycline hyclate was purchased from Heowns Biochem LLC. β-CD was purchased from Kmart (Tianjin) Chemical Technology Co., Ltd. PEI (Mw = 10 kDa) was purchased from Heowns Biochem LLC. PCL (Mw = 80 kDa) was purchased from Dalian Meilun Biotechnology Co., Ltd. Silver nitrate ($AgNO_3$) was purchased from Shanghai Aladdin Biochemical Technology Co., Ltd. *N*,*N*-Dimethylformamide (DMF) was purchased from Concord Technology (Tianjin) Co., Ltd. Hexafluoroisopropanol (HFIP) was purchased from Heowns Biochem Technologies LLC. All chemicals and solvents were used without further purification.

Preparation of β-CD-PEI. 6-*O*-(*p*-Toluenesulfonyl)-β-CD (6-OTs-β-CD) (3.867 g)[35] was dissolved in DMF (40 mL); after complete dissolution, a DMF (10 mL) solution of PEI (0.387 g) and triethylamine (0.364 g) was added. Then, the system was stirred at 70 °C for 24 h under an argon atmosphere and then cooled to room temperature. The precipitate was washed with DMF for three times, then dialyzed for 3 days, and dried to give β-CD-PEI.

Drug Loading Efficiency (DLE). A total of 0.6839 g Dox was mixed with 0.3637 g β-CD-PEI and stirred for 3 h. The reaction system was dialyzed for 2 h, and then the dialysate was taken out for UV−vis spectroscopy. The UV−vis absorption spectra were tested on a Shimadzu UV-3600 spectrophotometer equipped with a PTC-348WI temperature controller. According to the standard curve of Dox, the weight of the loaded drug was calculated to be 284.1 mg. The weight of the β-CD-PEI nanocarrier was 363.7 mg. Therefore, the DLE (DLE (wt %) = (weight of loaded drug/weight of nanocarrier) × 100%) was calculated to be 78.11%.

Preparation of Electrospun Nanofibrous Membranes. A total of 2.5 mL of 8 w/v % PVA solution containing 0.05 g Dox@β-CD-PEI was transferred to a 5 mL syringe with a 20 gauge (20 G) needle tip, and the spinning flow rate was 0.13 mm/min. A total of 4.5 mL of 11 w/v % PCL solution containing 0.0495 g $AgNO_3$ was transferred to another 5 mL syringe with a 23 G needle tip, and the spinning flow rate was 0.3 mm/min. Two kinds of spinning solution were electrospun at the same time; a high voltage of 30 kV was applied; and the distance between the collector coated with aluminum foil and the needle tip was 20 cm. The collector was rotated at 40 rpm. A dry PVA/Dox@β-CD-PEI/PCL/Ag nanofibrous membrane was collected directly from the aluminum foil-covered collector and stored at room

https://doi.org/10.1021/acs.biomac.1c01007
Biomacromolecules XXXX, XXX, XXX−XXX

temperature. According to the proportion of each substance added, it is calculated that the PVA/Dox@β-CD-PEI/PCL/Ag nanofibrous membrane contained 2.824% Dox and 4.051% Ag. For the PVA/Dox@β-CD-PEI/PCL nanofibrous membrane, 2.5 mL of 8 w/v % PVA solution containing 0.05 g Dox@β-CD-PEI and 4.5 mL of 11 w/v % PCL solution were electrospun at the same time. For the PVA/PCL/Ag nanofibrous membrane, 2.5 mL of 8 w/v % PVA solution and 4.5 mL of 11 w/v % PCL solution containing 0.0495 g $AgNO_3$ were electrospun at the same time. For the PVA/PCL nanofibrous membrane, 2.5 mL of 8 w/v % PVA solution and 4.5 mL of 11 w/v % PCL solution were electrospun at the same time.

Characterization of Electrospun Nanofibrous Membranes. ^{1}H NMR spectra were recorded on a Bruker Avance III 400 MHz nuclear magnetic resonance spectrometer. The surface microstructure of the nanofibrous membranes was acquired by using a scanning electron microscopy (SEM) (MERLIN Compact, Germany) with an acceleration voltage of 5 kV. All membranes were vacuum-dried and then coated with a thin layer of gold to increase their conductivity. Transmission electron microscopy (TEM) experiments were performed using a Philips Tecnai G2 F20 microscope operating. After the powder sample dissolved, the solution was dropped onto the copper grid to prepare the sample, while the electrospun fibrous sample was deposited directly on the copper grid about 3 s for TEM observation, so that the fibrous electrospun membrane is thin enough to allow electron beams to penetrate. Dynamic light scattering (DLS) measurements were recorded on a laser light scattering spectrometer (BI-200SM) equipped with a digital correlator (Turbo Corr.). A Fourier transform infrared spectrometer (FTIR) (Bruker-TENSOR II, Germany) was used to obtain the infrared spectra of samples between 4000 and 400 cm^{-1}. The stress−strain curves of the nanofibrous membranes were measured using a universal tensile tester (Instron-336, USA) with a load cell capacity of 10 N. The nanofibrous membranes were sectioned into rectangular strips of 4 × 1 cm^2, which were then fixed on the grips of the tester and allowed to elongate at an extension speed of 100 mm/min until they snapped. The surface chemical composition of the nanofibrous membranes was studied via X-ray photoelectron spectroscopy (XPS) performed on an instrument (Kratos Analytical Ltd.-Axis Ultra DLD) equipping with a monochromatized Al Kα X-ray source. Data were analyzed with CASAXPS software. Water contact angle was measured by using an optical contact angle (CA) meter (DSA100, Germany). In detail, the nanofibrous membranes were cut into rectangular blocks of 1 × 1 cm^2 and dried in a vacuum oven overnight. A water droplet (3 μL) was dropped on the surface of the membranes, and then an optical microscope was used to observe the state of water droplet and record the images.

Dox and Ag Release of Electrospun Nanofibrous Membrane. A 40 mL phosphate buffer saline (PBS) (pH = 7) was added to the beaker, and a dialysis bag (MWCO = 6000−8000) containing 20 mg PVA/Dox@β-CD-PEI/PCL/Ag nanofibrous membrane was put into the beaker which was maintained at 37 °C and 150 rpm. At 0.5, 1, 2, 4, 8, 17, 24, and 48 h, 1 mL solution outside the dialysis bag was collected to detect the release of Dox and Ag by UV−vis spectroscopy and ICP-OES, respectively.

Bacteriostatic Effect of Electrospun Nanofibrous Membranes. *E. coli* at the logarithmic phase was suspended to the concentration of 10^7 CFU mL^{-1}. Then, 200 μL of the *E. coli* suspension was spread on Luria-Bertani (LB) solid medium, evenly. The PVA/PCL, PVA/PCL/Ag, PVA/Dox@β-CD-PEI/PCL, and PVA/Dox@β-CD-PEI/PCL/Ag electrospun nanofibrous membranes cut into a circular disk shape (Φ_{cd} = 10 mm) were gently placed on the LB agar in a clockwise order and incubated at 37 °C. The antibacterial activity of the electrospun nanofibrous membranes was evaluated by measuring the diameters of its ZOI (d_{ZOI}) at 8, 20, and 30 h and calculating the corresponding normalized ZOI according to the obtained inhibition zone data (normalized ZOI = $(d_{ZOI}^2 - \Phi_{cd}^2)/\Phi_{cd}^2 \times 100\%$).[32]

In order to further verify the antibacterial activity of the electrospun nanofibrous membranes, the LB liquid medium turbidity assay was carried out. We cultured *E. coli* in LB liquid media for 24 h with and without the electrospun nanofibrous membranes and then visually observed the turbidity of the culture medium. The lower the turbidity, the fewer bacteria and the better the antibacterial effect of the electrospun nanofibrous membrane. Furthermore, an optical density at 600 nm (OD_{600nm}) of *E. coli* bacterial suspensions treated and untreated with electrospun nanofibrous membranes at 8 and 24 h was detected. Then, the bacteriostatic rate was obtained according to the optical density.

To evaluate the permeability of cell membranes, we treated the suspensions of *E. coli* with electrospun nanofibrous membranes at 37 °C for 4 h and stained them with propidium iodide (PI). The fluorescent dye PI is a nuclear staining reagent that shows red fluorescence after intercalation with DNA. PI cannot pass through living cell membranes, but it can pass through damaged cell membranes.

In Vivo Wound Healing Assay. Male Sprague−Dawley (SD) rats weighing about 250 g were used to evaluate the wound healing effect of PVA/Dox@β-CD-PEI/PCL/Ag. Rats were randomly divided into three groups: uninfected group, *Escherichia coli* DH5α (*E. coli*)-infected group, and MRSA-infected group. There were six rats in each group, three of which were using PVA/Dox@β-CD-PEI/PCL/Ag as dressing, and the other three were using gauze as dressing. After the SD rats were anesthetized, their backs were shaved, and then the areas were disinfected with 75% ethanol. Two full-thickness round skin wounds with a diameter of 1.5 cm were made on the dorsal side of each rat, one for observation of wound recovery and the other for pathological analysis. Subsequently, 50 μL of *E. coli* or MRSA suspension (1.0×10^8 CFU/mL) was used to cause infected wounds, and for the wounds of the uninfected group, 50 μL of sterile normal saline was used. Uninfected wounds refer to wounds without artificial infection, and the wounds are not necessarily completely sterile, which may be infected by bacteria in the natural environment. Two days later, the infected group was infected, and the wounds were covered with gauze or PVA/Dox@β-CD-PEI/PCL/Ag nanofibrous antibacterial membrane. Pictures of the wound location were taken to measure the size of the wound every 3−4 days. On the seventh day after wound infection, six wound tissues for pathological analysis were collected from each of the three groups: the uninfected group, *E. coli*-infected group, and MRSA infected group; three were from the gauze-treated rats, and the other three were from the PVA/Dox@β-CD-PEI/PCL/Ag nanofibrous antibacterial membrane-treated rats. All specimens were fixed in 4% paraformaldehyde solution for 2−3 days, and then the specimens were embedded in paraffin to prepare tissue sections with a thickness of 3−4 μm. Tissue sections were stained with H&E and imaged under an optical microscope. The animal experiments were approved by the Animal Care and Use Committee at Nankai University.

Ethical Statement. The animal experiments were performed in compliance with the guidelines of the Animal Care and Use Committee at Nankai University and the experiment guidelines of the College of Life Science at Nankai University. The committee approved all of the experiments.

RESULTS AND DISCUSSION

Characterization of Dox@β-CD-PEI. This study proposed the fabrication of bifunctional antibacterial membrane PVA/Dox@β-CD-PEI/PCL/Ag for wound dressing applications. First, β-CD-PEI was obtained by the synthetic route shown in Figure S1, and the specific operation process was presented in the methods part. Figure S2 shows the ^{1}H NMR spectra of β-CD-PEI in D_2O. The calculated degree of the substitution of β-CD on the PEI chain was 8% by integrating the peaks of the characteristic chemical shifts (δ) corresponding to PEI and β-CD. Dox is a broad-spectrum antibiotic, which has been reported to be encapsulated in the cavity of β-CD.[26] At the same time, the hydroxyl group of Dox can form hydrogen bonds with the hydroxyl group of β-CD and the amino group of PEI. Based on the reasons above, we used β-

https://doi.org/10.1021/acs.biomac.1c01007
Biomacromolecules XXXX, XXX, XXX−XXX

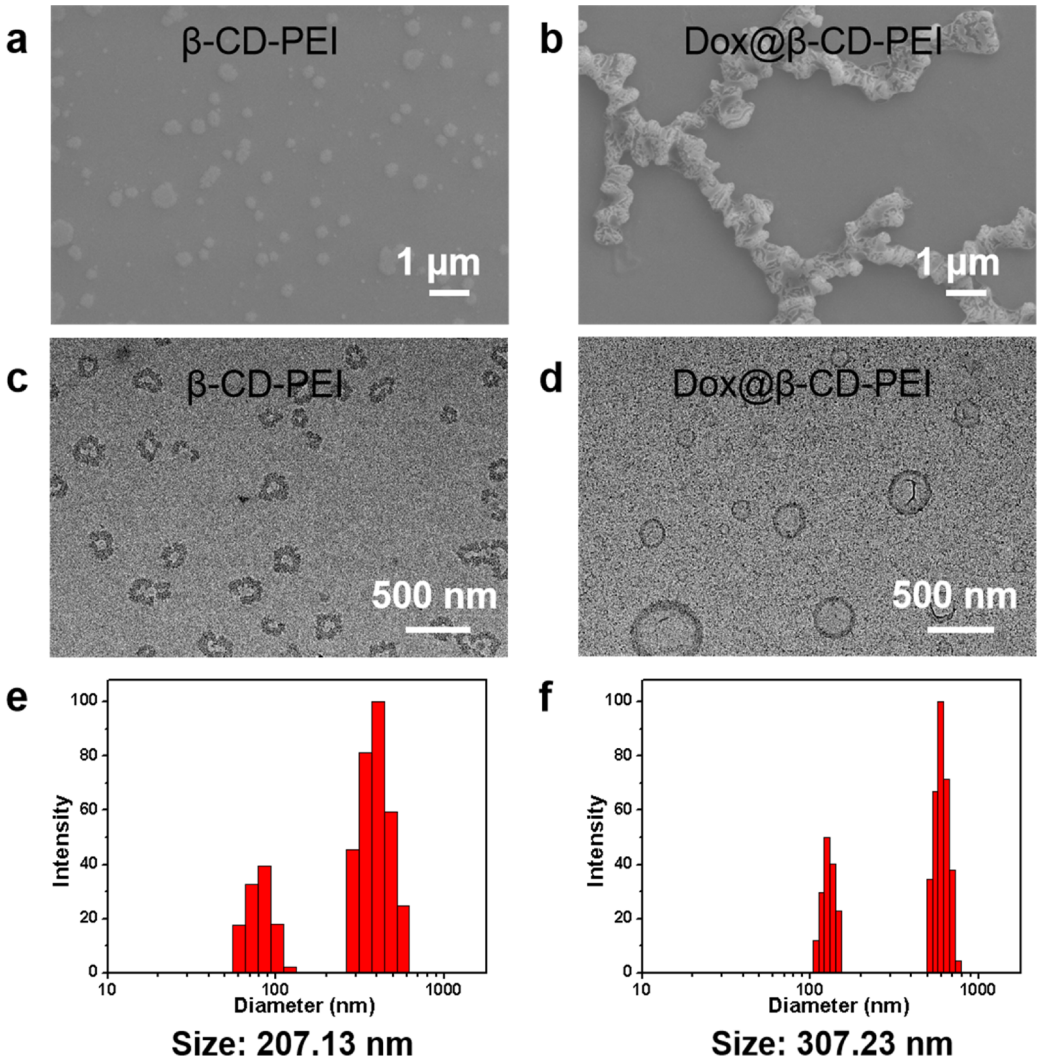

Figure 1. Characterization of the *β*-CD-PEI and Dox@*β*-CD-PEI. (a) SEM, (c) TEM, and (e) DLS of *β*-CD-PEI; (b) SEM, (d) TEM, and (f) DLS of Dox@*β*-CD-PEI.

CD-PEI to load Dox. According to the standard curve of Dox and the UV absorption curve of Dox@*β*-CD-PEI dialysate shown in Figure S3, the drug loading efficiency was calculated to be 78.11%.

The shape and size of *β*-CD-PEI and Dox@*β*-CD-PEI were investigated by scanning electron microscopy (SEM), transmission electron microscopy (TEM), and dynamic light scattering (DLS). Figure 1a,b presents the SEM images of *β*-CD-PEI and Dox@*β*-CD-PEI. It can be seen that *β*-CD-PEI was a nanoparticle about 200 nm and Dox@*β*-CD-PEI was a dendritic structure composed of nanoparticles about 300 nm. TEM images in Figure 1c,d shows that *β*-CD-PEI was an irregular hollow vesicle about 200 nm, while Dox@*β*-CD-PEI was a spherical vesicle about 300 nm in size. The DLS of *β*-CD-PEI and Dox@*β*-CD-PEI given in Figure 1e,f further proved that the average particle size of *β*-CD-PEI was about 200 nm, while the average particle size of Dox@*β*-CD-PEI was approximately 300 nm.

Figure S4 shows the Fourier transform infrared spectrometry (FTIR) spectra of PEI, *β*-CD-PEI, and Dox@*β*-CD-PEI. Compared with the normal primary amine peak, the broad peak at 3276 cm^{-1} had no obvious double peak shape and moved to the direction of the low wavenumber, indicating that there was not only a combined NH_2 structure but also a NH structure in the compound. The stretching vibration peaks of CH_2 were at 2931 and 2807 cm^{-1}; the in-plane bending vibration peaks of CH_2 were at 1454 cm^{-1}; the NH bending vibration peaks of secondary amine were at 1590 cm^{-1}; and the C−N stretching vibration peaks of primary amine and secondary amine were at 1349−1044 cm^{-1}.[36] For *β*-CD-PEI, in addition to the characteristic peaks of PEI, the IR bands around 1567, 1152, 1028, and 937 cm^{-1} were due to the glucopyranose ring stretching vibration band, the coupled ν(C−C/C−O) stretching vibration, antisymmetric glycosidic νa(C−O−C) vibrations, and the R-1,4-bond skeleton vibration of *β*-CD.[37] For Dox@*β*-CD-PEI, in addition to the characteristic peaks of PEI and *β*-CD, the peak at 1667 cm^{-1} was assigned to C═O, the peak at 706 cm^{-1} was assigned to C═C, the peaks at 1614 cm^{-1}, 1580 cm^{-1}, and 1455 cm^{-1} were assigned to the vibration of the benzene ring skeleton, and the peak at 575 cm^{-1} were assigned to the deformation vibration of the benzene ring skeleton. The above results prove that Dox was loaded on *β*-CD-PEI.

Characterization of Electrospun Nanofibrous Membranes. Figure S5 presents the SEM images of the four nanofibrous membranes prepared by electrospinning. Figure

https://doi.org/10.1021/acs.biomac.1c01007
Biomacromolecules XXXX, XXX, XXX−XXX

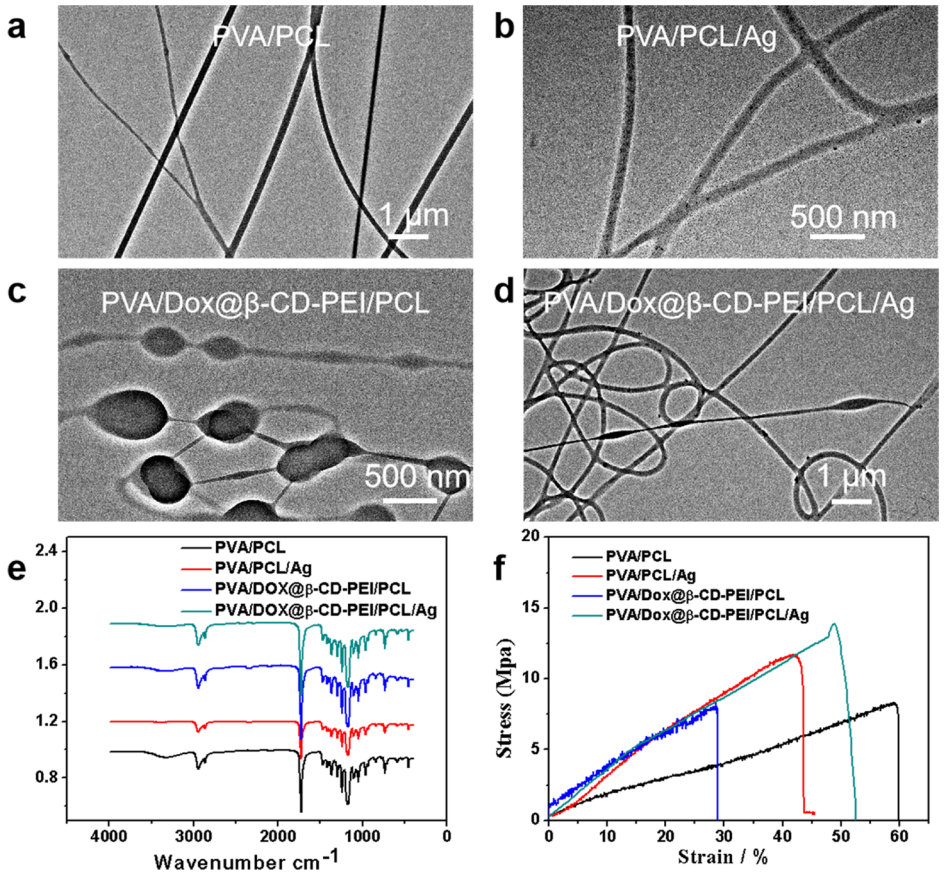

Figure 2. Characterization of the nanofibrous membranes. (a–d) TEM, (e) FTIR spectra, and (f) stress–strain curves of PVA/PCL, PVA/PCL/Ag, PVA/Dox@*β*-CD-PEI/PCL, and PVA/Dox@*β*-CD-PEI/PCL/Ag.

S5a shows the SEM image of PVA/PCL. It can be clearly seen that there were two types of fibers with different sizes. Fibers with the larger diameter were PCL fibers, while the others with the smaller diameter were PVA fibers. The other three membranes shown in Figure S5b–d also had similar morphologies.

In order to obtain more morphology information, TEM was used to corroborate and supplement the SEM, as shown in Figure 2a–d. Consistent with the SEM results, two kinds of nanofibers with different diameters also appeared in TEM images. From Figure 2b,d, we can see that many small black nanoparticles were scattered in the PCL nanofibers, which were Ag. Comparing PVA and PVA/Dox@*β*-CD-PEI fibers, it can be seen that PVA was a uniform and smooth nanofiber, while when Dox@*β*-CD-PEI was added to PVA, fibers containing a large number of beads were obtained. Figure 2e shows the FT-IR spectra of the four nanofibrous membranes. The stretching vibration peaks of C–H were at 2943 and 2866 cm^{-1}; the bending vibration of C–H were in the 1471–1365 cm^{-1} region; the peak at 1723 cm^{-1} was assigned to C═O; and the peaks in the 1294–1165 cm^{-1} region were the characteristic peaks of C–O–C. These above results indicated that PCL nanofibers were successfully constructed.[38] The peak at 3330 cm^{-1} was assigned to O–H of PVA. The infrared spectra of the four membranes were very similar because the signals of the characteristic peaks of PCL were very strong; thus, the signals of some other functional groups can be easily masked and are difficult to be detected. The stress–strain curves of PVA/PCL, PVA/PCL/Ag, PVA/Dox@*β*-CD-PEI/PCL, and PVA/Dox@*β*-CD-PEI/PCL/Ag are shown in Figure 2f. The PVA/PCL membrane showed a Young's modulus of 16.29 MPa, a yield strength of 8.365 MPa, and an elongation at break of 59.08%. The PVA/PCL/Ag membrane showed a Young's modulus of 32.52 MPa, a yield strength of 11.73 MPa, and an elongation at break of 41.76%. The PVA/Dox@*β*-CD-PEI/PCL membrane showed a Young's modulus of 28.17 MPa, a yield strength of 8.302 MPa, and an elongation at break of 28.63%. The PVA/Dox@*β*-CD-PEI/PCL/Ag membrane showed a Young's modulus of 33.64 MPa, a yield strength of 13.87 MPa, and an elongation at break of 48.82%. These membranes could undergo a significant deformation rather than sudden fracture during stretching. Their mechanical properties are similar with or even better than some other electrospun membranes reported.[39,40] Such mechanical performance is conducive to their further application into the wound dressing field.

X-ray photoelectron spectroscopy (XPS) measurements were carried out to investigate the surface chemical compositions of the electrospun nanofibrous membranes (Figure 3). The XPS spectrum of the PVA/PCL membrane showed peaks assignable to C (283 eV) and O (530 eV); PVA/PCL/Ag showed peaks assignable to C (283 eV), Ag 3d (366 eV), and O (530 eV); PVA/Dox@*β*-CD-PEI/PCL showed peaks assignable to C (283 eV), N (392 eV), and O (530 eV); and PVA/Dox@*β*-CD-PEI/PCL/Ag showed peaks assignable to C (283 eV), Ag 3d (366 eV), N (392 eV), and O (530 eV). As shown in Figure 3e,f, the binding energy of Ag 3d peaks of 365.7 and 371.7 were attributed to Ag $3d_{5/2}$ and Ag $3d_{3/2}$ with an orbit separation of 6 eV. A peak fitting procedure was used to individuate the two spin–orbit pairs. Ag $3d_{5/2}$

https://doi.org/10.1021/acs.biomac.1c01007
Biomacromolecules XXXX, XXX, XXX–XXX

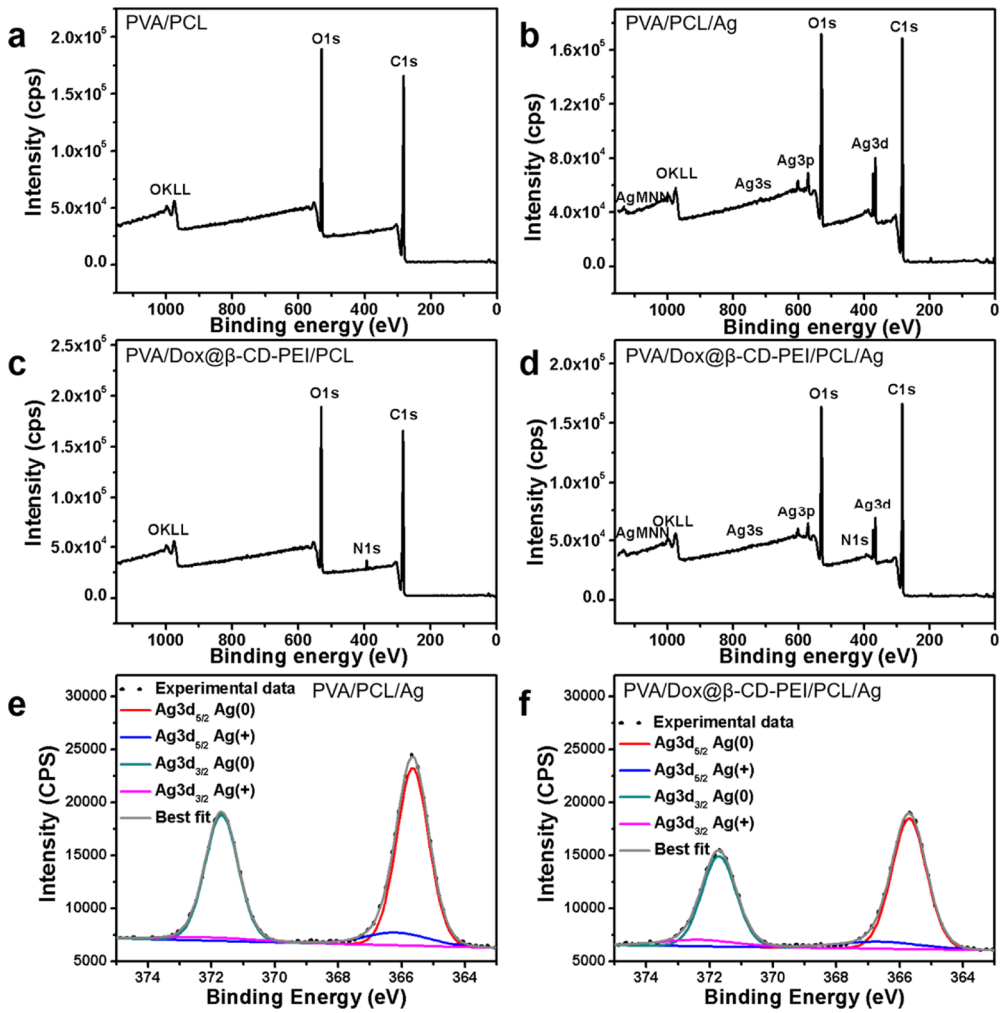

Figure 3. XPS spectra of (a) PVA/PCL, (b) PVA/PCL/Ag, (c) PVA/Dox@*β*-CD-PEI/PCL, and (d) PVA/Dox@*β*-CD-PEI/PCL/Ag. XPS Ag 3d spectra of (e) PVA/PCL/Ag and (f) PVA/Dox@*β*-CD-PEI/PCL/Ag.

(365.65 eV) and Ag $3d_{3/2}$ (371.68 eV) were attributed to the metallic Ag signal. In addition, Ag $3d_{5/2}$ (366.17 eV) and Ag $3d_{3/2}$ (372.09 eV) were assigned to the positively charged Ag. XPS results showed that most of the Ag in the PVA/PCL/Ag and PVA/Dox@*β*-CD-PEI/PCL/Ag nanofibrous membranes exist in the form of Ag^0, and only a small part of Ag exist in the form of Ag^+. Adding Ag^+ to the spinning solution can produce AgNP in situ, which is consistent with the previous reports.[32,41]

The wettability of water droplets on electrospun nanofibrous membranes was observed by an optical microscope. The optical images are shown in Figure S6. PCL was hydrophobic with a contact angle of 120°, approximately. PVA was hydrophilic; water could be instantly absorbed when contacted with PVA. For the electrospun membranes of PVA/PCL, PVA/PCL/Ag, PVA/Dox@*β*-CD-PEI/PCL, and PVA/Dox@*β*-CD-PEI/PCL/Ag, water droplets could be completely absorbed in 1 min. The hydrophilic electrospun nanofibrous membranes with a net-like structure are conducive to use as wound dressing because they could absorb the exudate from the wound surface and prevent the exudate from spreading and seeping back to the normal skin around the wound.

The release profiles of Dox and Ag from the PVA/Dox@*β*-CD-PEI/PCL/Ag nanofibrous membrane were tested in PBS solution at different times. The release of Dox was measured by ultraviolet−visible (UV−vis) spectroscopy, and the release of Ag was measured by an inductively coupled plasma optical emission spectrometer (ICP-OES). The rates of Dox release (Figure S7, Figure 4a,c) and Ag release (Figure 4b,d) from the nanofibrous membrane were significantly different. Dox was released from the nanofibrous membrane as a burst release (89%) in the first 0.5 h and had a cumulative release reaching approximately 97% in 1 h and approximately 99% in 2 days. However, the release of Ag from the nanofibrous membrane was very slow, the release rate was about 0.59% in the first 0.5 h and the cumulative release reached only approximately 2.01% in 1 h and 6.27% in 2 days. The faster Dox release was due to the fact that Dox was encapsulated in water-soluble PVA nanofibers. However, Ag was encapsulated in non-water-soluble and hydrophobic PCL, so its release rate was very slow. In summary, the burst release of Dox can kill bacteria quickly and the prolonged release of Ag can achieve a long-term bactericidal and antibacterial effect, which is completely consistent with our original intention in this article. It makes sense to integrate the burst release and sustained release into one system.[42] Figure S8 revealed the in vitro degradation of the PVA/Dox@*β*-CD-PEI/PCL/Ag nanofibrous membrane in PBS solutions at pH 7.0 for 18 days. No fiber-like structure was observed, suggesting that it possessed good biodegradability.[43]

https://doi.org/10.1021/acs.biomac.1c01007
Biomacromolecules XXXX, XXX, XXX−XXX

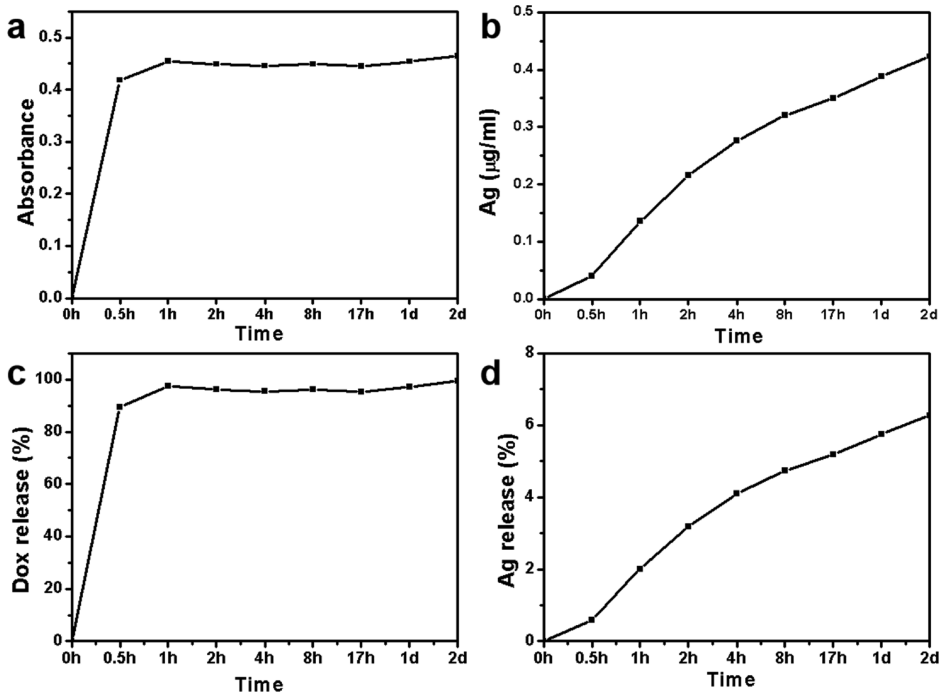

Figure 4. Release profiles of (a, c) Dox and (b, d) Ag from PVA/Dox@*β*-CD-PEI/PCL/Ag nanofibrous membrane in PBS at 37 °C.

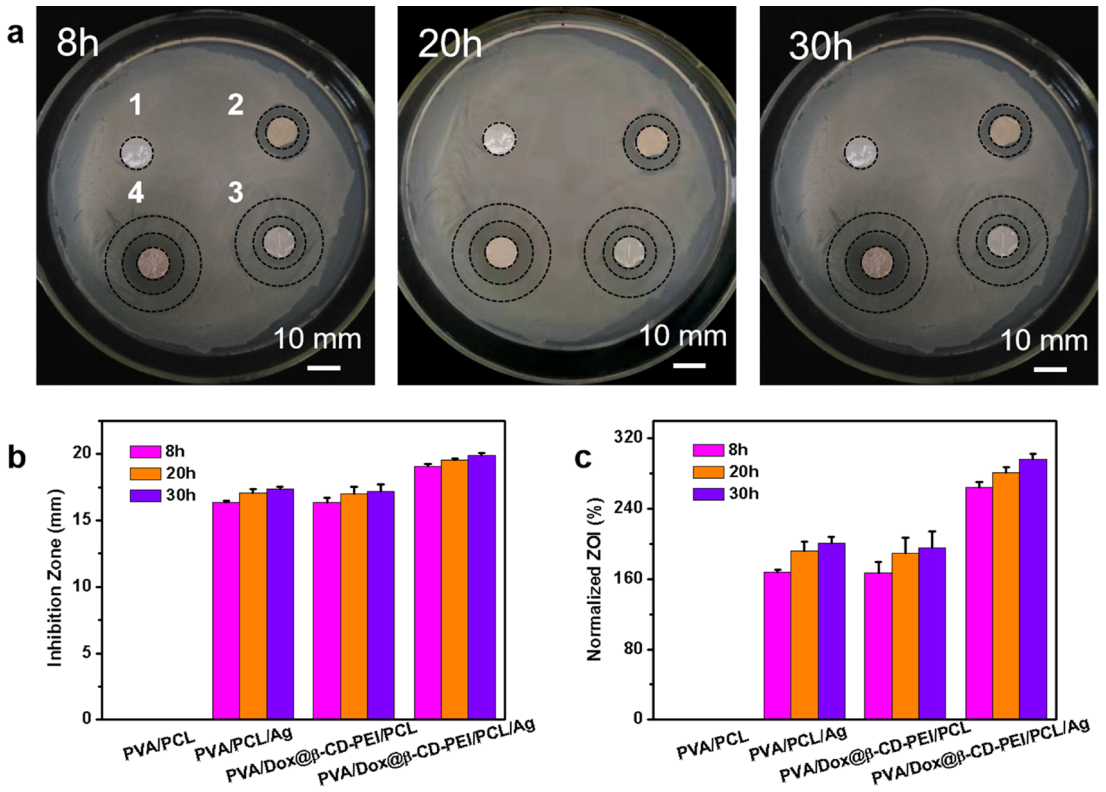

Figure 5. Antibacterial activity of nanofibrous membranes. (a) Images showing the inhibition zone of the nanofibrous membranes against *E. coli* after 8, 20, and 30 h cultivation on agar; (1) PVA/PCL; (2) PVA/PCL/Ag; (3) PVA/Dox@*β*-CD-PEI/PCL; (4) PVA/Dox@*β*-CD-PEI/PCL/Ag. (b) Diameter of the inhibition zone and (c) statistics of the normalized ZOI.

Bacteriostatic Effect of Electrospun Nanofibrous Membranes. The in vitro antibacterial activity of the four nanofibrous membranes were evaluated by the size of the inhibition zone (ZOI) shown in Figure 5. ZOI describes the area of sterile zone of nanofibrous membranes, which corresponds to the antibacterial ability of nanofibrous membranes. As a result, the PVA/PCL nanofibrous membrane had no ZOI at different times. The PVA/PCL/Ag nanofibrous membrane showed a great antibacterial impact against *E. coli* with a diameter zone of inhibition of 16.37 mm at 8 h, 17.09

https://doi.org/10.1021/acs.biomac.1c01007
Biomacromolecules XXXX, XXX, XXX−XXX

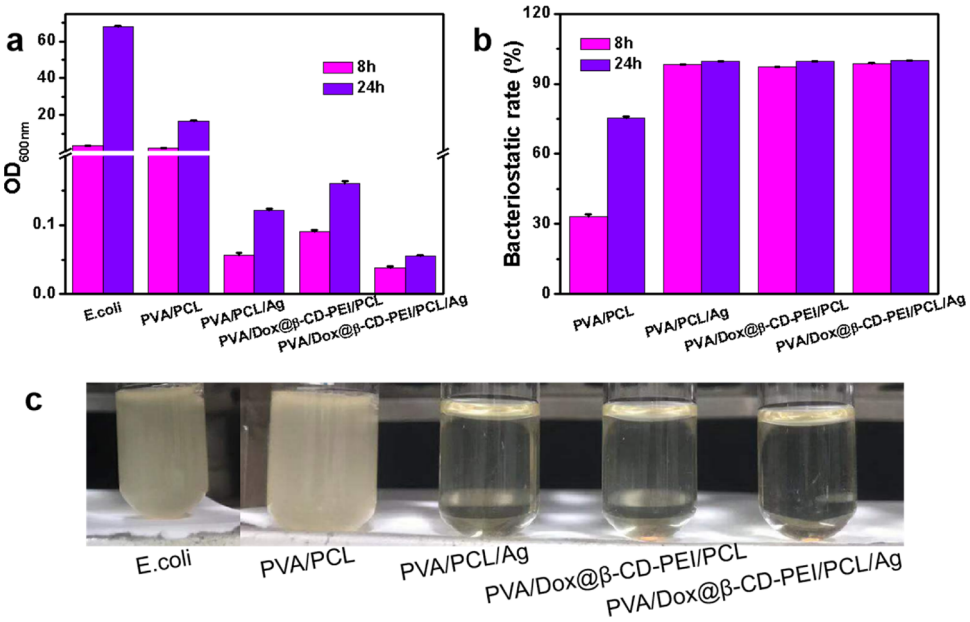

Figure 6. Antibacterial activity of nanofibrous membranes. (a) Optical density at 600 nm (OD_{600nm}) of *E. coli* treated and untreated with nanofibrous membranes after 8 and 24 h cultivation, (b) bacteriostatic rate calculated corresponding to optical density based on bacteria count, and (c) LB liquid medium turbidity assays.

mm at 20 h, and 17.35 mm at 30 h. Similarly, the PVA/Dox@*β*-CD-PEI/PCL nanofibrous membrane could effectively inhibit the growth of *E. coli* with a diameter zone of inhibition of 16.35 mm at 8 h, 17.01 mm at 20 h and 17.19 mm at 30 h. Additionally, *E. coli* was strongly inhibited by the PVA/Dox@*β*-CD-PEI/PCL/Ag nanofibrous membrane and the ZOI reached 19.07 mm at 8 h, 19.52 mm at 20 h, and 19.90 mm at 30 h. The normalized ZOI is shown in Figure 5c. It can be seen that the normalized ZOI of the PVA/Dox@*β*-CD-PEI/PCL/Ag nanofibrous membrane was the largest, which was 263.7, 281.2, and 296.2% at 8, 20, and 30 h, respectively. The normalized ZOI is larger than that of some other reported antibacterial materials.[32,33,44] The above results showed that the PVA/Dox@*β*-CD-PEI/PCL/Ag nanofibrous membrane had the best antibacterial effect.

In addition to ZOI, there was a zone with significantly less bacteria outside the ZOI of PVA/Dox@*β*-CD-PEI/PCL and PVA/Dox@*β*-CD-PEI/PCL/Ag nanofibrous membranes. For PVA/Dox@*β*-CD-PEI/PCL, the diameter of this less bacteria zone was 27.58 mm at 8 h, 28.42 mm at 20 h, and 29.29 mm at 30 h. For PVA/Dox@*β*-CD-PEI/PCL/Ag, the diameter of this less bacteria zone was 29.95 mm at 8 h, 30.14 mm at 20 h and 31.29 mm at 30 h.

E. coli was incubated with four nanofibrous membranes for 8 and 24 h, and then the OD_{600} values were measured. By comparing with the single *E. coli*, it was found that PVA/PCL/Ag, PVA/Dox@*β*-CD-PEI/PCL, and PVA/Dox@*β*-CD-PEI/PCL/Ag nanofibrous membranes could inhibit the growth of bacteria very well, and even PVA/PCL had certain antibacterial ability (Figure 6). When incubated with *E. coli* for 8 h, the bacteriostatic rates of PVA/PCL, PVA/PCL/Ag, PVA/Dox@*β*-CD-PEI/PCL, and PVA/Dox@*β*-CD-PEI/PCL/Ag nanofibrous membranes were 33.18, 98.24, 97.19, and 98.82%, respectively. Furthermore, when incubated with *E. coli* for 24 h, the bacteriostatic rates of PVA/PCL, PVA/PCL/Ag, PVA/Dox@*β*-CD-PEI/PCL, and PVA/Dox@*β*-CD-PEI/PCL/Ag nanofibrous membranes were 75.32, 99.82, 99.76, and 99.92%, respectively. In order to visually observe the antibacterial activity of nanofibrous membranes, we also carried out the Luria-Bertani (LB) liquid medium turbidity assay. We cultured *E. coli* in LB liquid medium alone for 24 h, and the mixture became turbid. The higher the turbidity, the more bacteria, indicating that bacteria proliferate rapidly in the medium. However, when *E. coli* was cultured in LB liquid medium with PVA/PCL/Ag, PVA/Dox@*β*-CD-PEI/PCL, and PVA/Dox@*β*-CD-PEI/PCL/Ag nanofibrous membranes for 24 h, the mediums remained transparent, indicating that few *E. coli* proliferated, reflecting that these nanofibrous membranes had very excellent antibacterial effect.

To further understand the antibacterial mechanism, the permeability of *E. coli* cell membranes in the presence of nanofibrous membranes was evaluated. We incubated the suspensions of *E. coli* with nanofibrous membranes at 37 °C for 4 h and stained them with PI. Fluorescence images exhibited in Figure S9 show that the fluorescence of *E. coli* treated with PVA/PCL/Ag, PVA/Dox@*β*-CD-PEI/PCL, and PVA/Dox@*β*-CD-PEI/PCL/Ag nanofibrous membranes increased, indicating that the permeability of *E. coli* cell membranes was increased. When treated with PVA/PCL, no fluorescence was observed in *E. coli*, which proved that *E. coli* cell membranes were not damaged. Therefore, the possible antimicrobial mechanism of the nanofibrous membranes is that the antibacterial active substance in the nanofibrous membranes can induce disruption to bacterial membrane and cause intracellular components to leak, leading to the death of the bacteria.

In Vivo Wound Healing Assay. The gauze that is widely used clinically has no antibacterial properties. Therefore, through in vivo experiments, the effect of PVA/Dox@*β*-CD-PEI/PCL/Ag nanofibrous membrane as a dressing on wound healing was further studied, including uninfected wounds, wounds infected by Gram-negative bacteria *E. coli*, and wounds infected by Gram-positive bacteria MRSA. Representative photos of the wound healing process are shown in Figure 7a–

https://doi.org/10.1021/acs.biomac.1c01007
Biomacromolecules XXXX, XXX, XXX−XXX

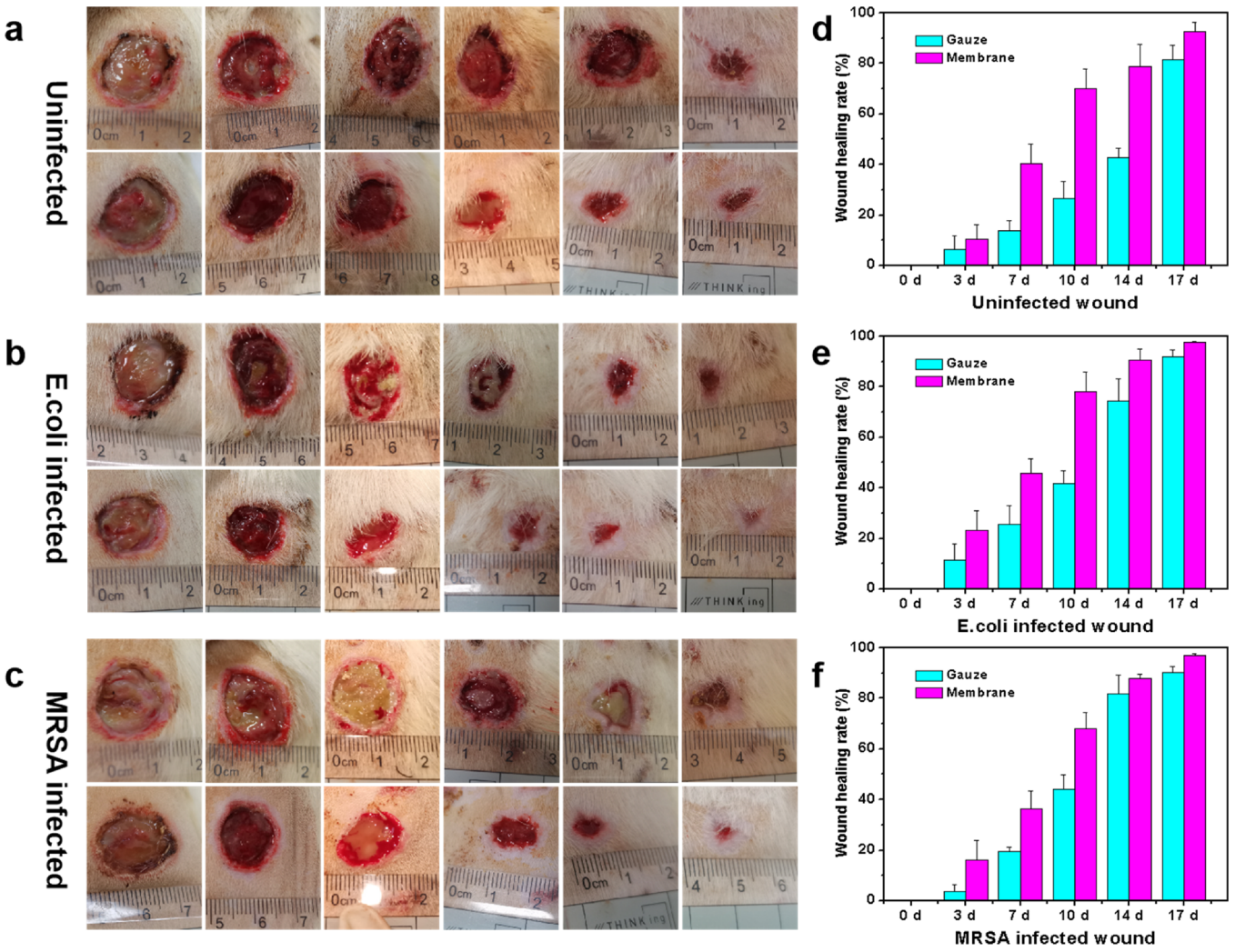

Figure 7. Promotion of wound healing by PVA/Dox@β-CD-PEI/PCL/Ag in vivo. Representative images of the (a) uninfected, (b) *E. coli*-infected, and (c) MRSA-infected wounds following surgery (0 days), and after 3, 7, 10, 14, and 17 days of treatment. In each group, the top row depicts wounds treated with gauze, and the bottom row depicts wounds treated with PVA/Dox@β-CD-PEI/PCL/Ag dressing. Statistics of the healing rates of (d) uninfected, (e) *E. coli*-infected, and (f) MRSA-infected wounds in (a–c).

c. In each group, significant differences were observed between wounds treated with the PVA/Dox@β-CD-PEI/PCL/Ag nanofibrous membrane and gauze. Not only uninfected wounds but even wounds infected by *E. coli* and MRSA showed significantly accelerated wound closure after treatment with the PVA/Dox@β-CD-PEI/PCL/Ag nanofibrous membrane. The measured wound area and wound healing rate during the entire treatment period are quantified in Figures S10–S12 and Figure 7d–f. In Figures S10–S12, Gauze1, Gauze2, and Gauze3 refer to three parallel test groups using gauze as wound dressing, and Membrane1, Membrane2, and Membrane3 refer to three parallel test groups using the PVA/Dox@β-CD-PEI/PCL/Ag nanofibrous membrane as wound dressing. The wound treated with the nanofibrous membrane showed significantly faster recovery than that treated with gauze, and the wound healing rates in different days were higher than that in the gauze treatment group. The wound healing rates of the gauze treatment group on 3, 7, 10, 14, and 17 days were 6.3, 13.6, 26.5, 42.8, and 81.5%, respectively, while those of the nanofibrous membrane treatment group were as high as 10.4, 40.4, 70.0, 78.9, and 92.8%. More importantly, the PVA/Dox@β-CD-PEI/PCL/Ag nanofibrous membrane significantly promoted the healing of wounds infected by *E. coli* and MRSA, proving its excellent antibacterial effect on infected wounds. The wound healing rates of *E. coli* infected wounds in the gauze treatment group at 3, 7, 10, 14, and 17 days were 11.2, 25.7, 41.8, 74.4, and 92.0%, respectively, while those of the nanofibrous membrane treatment group were as high as 23.2, 45.6, 78.0, 90.7, and 97.6%. The wound healing rates of MRSA infected wounds in the gauze treatment group at 3, 7, 10, 14, and 17 days were 3.6, 19.4, 44.1, 81.9, and 90.2%, respectively, while those of the nanofibrous membrane treatment group were as high as 16.2, 36.2, 68.0, 87.8, and 97.1%.

Hematoxylin and eosin (H&E) is used for the histomorphological examination of wound healing (Figure 8 and Figure S13).

Compared with uninfected wounds, more inflammatory cells were found in wounds infected with *E. coli* and MRSA. More inflammatory cells were observed in wounds infected by MRSA than in wounds infected by *E. coli*, indicating that MRSA infections may be more harmful and difficult to cure. After treatment with the PVA/Dox@β-CD-PEI/PCL/Ag nanofibrous membrane, the number of inflammatory cells

https://doi.org/10.1021/acs.biomac.1c01007
Biomacromolecules XXXX, XXX, XXX–XXX

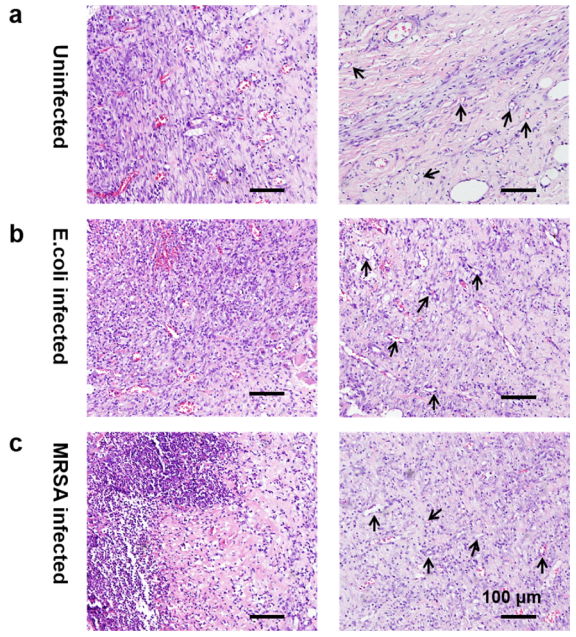

Figure 8. Histopathologic profiles of (a) uninfected, (b) *E. coli*-infected, and (c) MRSA-infected wounds. In each group, the left line depicts wounds treated with gauze, and the right line depicts wounds treated with PVA/Dox@β-CD-PEI/PCL/Ag dressing. Arrows indicate neovascularization. All scale bars are 100 μm.

decreased significantly and the number of neovascularization increased. Therefore, the PVA/Dox@β-CD-PEI/PCL/Ag nanofibrous membrane as a wound dressing has a significant acceleration effect on the wound healing process of uninfected, *E. coli*-infected, and MRSA-infected wounds. The excellent antibacterial and wound healing properties of the PVA/Dox@β-CD-PEI/PCL/Ag nanofibrous membrane means that this new material has the potential to be used as a clinical skin regeneration dressing, especially for wounds with bacterial infections.

CONCLUSIONS

In summary, a PVA/Dox@β-CD-PEI/PCL/Ag electrospun nanofibrous membrane had been successfully prepared through a simple and facile method. Ag, antibiotics, and cationic polymer antibacterial active substances were combined to act synergistically on bacteria. Dox was released from the nanofibrous membrane as a burst release (89%) in the first 0.5 h. However, the cumulative release of Ag reached only approximately 6.27% in 2 days. The normalized ZOI of the PVA/Dox@β-CD-PEI/PCL/Ag nanofibrous membrane was the largest, which was 263.7 and 296.2% at 8 and 30 h, respectively. The bacteriostatic rate of the PVA/Dox@β-CD-PEI/PCL/Ag nanofibrous membrane against *E. coli* was 98.82% at 8 h and 99.92% at 24 h. This article proves that the PVA/Dox@β-CD-PEI nanofibers will burst antimicrobial active drugs to kill bacteria quickly, while the prolonged release of Ag in PCL/Ag can kill bacteria and inhibit their growth for a long time. When used as wound dressing, the PVA/Dox@β-CD-PEI/PCL/Ag nanofibrous membrane showed significantly accelerated wound closure toward uninfected wounds, *E. coli*-infected wounds, and MRSA-infected wounds. It is conceivable that this dual-function membrane has wide applicability and versatility and is expected to be used in the clinical treatment of wound infections.

ASSOCIATED CONTENT

Supporting Information

The Supporting Information is available free of charge at https://pubs.acs.org/doi/10.1021/acs.biomac.1c01007.

Synthetic route of β-CD-Modified PEI, ^{1}H NMR spectra of β-CD-PEI, UV absorption curve, FTIR spectra, SEM, optical images of a water droplet on the nanofibrous membrane, release profiles of Dox, confocal laser scanning microscopy (CLSM) images, wound area measurements, wound healing rate, and H&E staining image (PDF)

AUTHOR INFORMATION

Corresponding Author

Yu Liu − *College of Chemistry, State Key Laboratory of Elemento-Organic Chemistry, Nankai University, Tianjin 300071, P. R. China;* orcid.org/0000-0001-8723-1896; Email: yuliu@nankai.edu.cn

Authors

Wenshi Xu − *College of Chemistry, State Key Laboratory of Elemento-Organic Chemistry, Nankai University, Tianjin 300071, P. R. China*

Yong Chen − *College of Chemistry, State Key Laboratory of Elemento-Organic Chemistry, Nankai University, Tianjin 300071, P. R. China*

Bing Zhang − *College of Chemistry, State Key Laboratory of Elemento-Organic Chemistry, Nankai University, Tianjin 300071, P. R. China*

Wenwen Xu − *College of Chemistry, State Key Laboratory of Elemento-Organic Chemistry, Nankai University, Tianjin 300071, P. R. China*

Jie Niu − *College of Chemistry, State Key Laboratory of Elemento-Organic Chemistry, Nankai University, Tianjin 300071, P. R. China*

Complete contact information is available at: https://pubs.acs.org/10.1021/acs.biomac.1c01007

Author Contributions

Y.L., Y.C., and W.-S.X. conceived and designed the experiments. W.-S.X. conducted all experiments except the in vitro antibacterial experiments. B.Z., W.-W.X., and J.N. conducted the in vitro antibacterial experiments. W.-S.X. wrote the main manuscript. Y.L. supervised the work and edited the manuscript. All authors analyzed and discussed the results and reviewed the manuscript.

Funding

This work was financially supported by the National Natural Science Foundation of China (grant nos. 22131008, 21772099, 21861132001, and 21971127).

Notes

The authors declare no competing financial interest.

REFERENCES

(1) Hu, B.; Owh, C.; Chee, P.; Leow, W.; Liu, X.; Wu, Y.-L.; Guo, P.; Loh, X. J.; Chen, X. Supramolecular hydrogels for antimicrobial therapy. *Chem. Soc. Rev.* **2018**, *47*, 6917−6929.

(2) Agnello, S.; Brand, M.; Chellat, M. F.; Gazzola, S.; Riedl, R. A Structural View on Medicinal Chemistry Strategies against Drug Resistance. *Angew. Chem., Int. Ed.* **2019**, *58*, 3300−3345.

(3) Wheatley, R.; Caballero, J. D.; Kapel, N.; de Winter, F. H. R.; Jangir, P.; Quinn, A.; del Barrio-Tofino, E.; Lopez-Causape, C.;

Hedge, J.; Torrens, G.; Van der Schalk, T.; Xavier, B. B.; Fernandez-Cuenca, F.; Arenzana, A.; Recanatini, C.; Timbermont, L.; Sifakis, F.; Ruzin, A.; Ali, O.; Lammens, C.; Goossens, H.; Kluytmans, J.; Kumar-Singh, S.; Oliver, A.; Malhotra-Kumar, S.; MacLean, C. Rapid evolution and host immunity drive the rise and fall of carbapenem resistance during an acute Pseudomonas aeruginosa infection. *Nat. Commun.* **2021**, *12*, 2460.

(4) Mankoci, S.; Ewing, J.; Dalai, P.; Sahai, N.; Barton, H. A.; Joy, A. Bacterial Membrane Selective Antimicrobial Peptide-Mimetic Polyurethanes: Structure-Property Correlations and Mechanisms of Action. *Biomacromolecules* **2019**, *20*, 4096−4106.

(5) Peng, C.; Vishwakarma, A.; Mankoci, S.; Barton, H. A.; Joy, A. Structure-Activity Study of Antibacterial Poly(ester urethane)s with Uniform Distribution of Hydrophobic and Cationic Groups. *Biomacromolecules* **2019**, *20*, 1675−1682.

(6) Lakemeyer, M.; Zhao, W.; Mandl, F. A.; Hammann, P.; Sieber, S. A. Thinking Outside the Box-Novel Antibacterials To Tackle the Resistance Crisis. *Angew. Chem., Int. Ed.* **2018**, *57*, 14440−14475.

(7) Ding, X.; Duan, S.; Ding, X.; Liu, R.; Xu, F.-J. Versatile Antibacterial Materials: An Emerging Arsenal for Combatting Bacterial Pathogens. *Adv. Funct. Mater.* **2018**, *28*, 1802140.

(8) Wang, L.; Gao, F.; Wang, A.; Chen, X.; Li, H.; Zhang, X.; Zheng, H.; Ji, R.; Li, B.; Yu, X.; Liu, J.; Gu, Z.; Chen, F.; Chen, C. Defect-Rich Adhesive Molybdenum Disulfide/rGO Vertical Heterostructures with Enhanced Nanozyme Activity for Smart Bacterial Killing Application. *Adv. Mater.* **2020**, *32*, 2005423.

(9) Peng, S.; He, Q.; Vargas-Zuniga, G. I.; Qin, L.; Hwang, I.; Kim, S. K.; Heo, N. J.; Lee, C.-H.; Dutta, R.; Sessler, J. L. Strapped calix 4 pyrroles: from syntheses to applications. *Chem. Soc. Rev.* **2020**, *49*, 865−907.

(10) Yang, C.; Inoue, Y. Supramolecular photochirogenesis. *Chem. Soc. Rev.* **2014**, *43*, 4123−4143.

(11) Li, Z.; Liu, X.; Wang, G.; Li, B.; Chen, H.; Li, H.; Zhao, Y. Photoresponsive supramolecular coordination polyelectrolyte as smart anticounterfeiting inks. *Nat. Commun.* **2021**, *12*, 1363.

(12) Wang, K.; Jordan, J. H.; Velmurugan, K.; Tian, X.; Zuo, M.; Hu, X.-Y.; Wang, L. Role of Functionalized Pillararene Architectures in Supramolecular Catalysis. *Angew. Chem., Int. Ed.* **2021**, *60*, 9205−9214.

(13) Sun, G.; He, Z.; Hao, M.; Zuo, M.; Xu, Z.; Hu, X.-Y.; Zhu, J.-J.; Wang, L. Dual acid-responsive bola-type supramolecular vesicles for efficient intracellular anticancer drug delivery. *J. Mater. Chem. B* **2019**, *7*, 3944−3949.

(14) Lim, W. Q.; Phua, S. Z. F.; Chen, H.; Zhao, Y. An oxaliplatin(iv) prodrug-based supramolecular self-delivery nanocarrier for targeted colorectal cancer treatment. *Chem. Commun.* **2018**, *54*, 12762−12765.

(15) Li, L.; Lin, Q.; Tang, M.; Tsai, E. H. R.; Ke, C. An Integrated Design of a Polypseudorotaxane-Based Sea Cucumber Mimic. *Angew. Chem., Int. Ed.* **2021**, *60*, 10186−10193.

(16) Liu, Z.; Dai, X.; Sun, Y.; Liu, Y. Organic supramolecular aggregates based on water-soluble cyclodextrins and calixarenes. *Aggregate* **2020**, *1*, 31−44.

(17) Wang, J.; Feng, L.; Yu, Q.; Chen, Y.; Liu, Y. Polysaccharide-Based Supramolecular Hydrogel for Efficiently Treating Bacterial Infection and Enhancing Wound Healing. *Biomacromolecules* **2021**, *22*, 534−539.

(18) Li, X.; Bai, H.; Yang, Y.; Yoon, J.; Wang, S.; Zhang, X. Supramolecular Antibacterial Materials for Combatting Antibiotic Resistance. *Adv. Mater.* **2019**, *31*, 1805092.

(19) Nandi, N.; Gayen, K.; Ghosh, S.; Bhunia, D.; Kirkham, S.; Sen, S. K.; Ghosh, S.; Hamley, I. W.; Banerjee, A. Amphiphilic Peptide-Based Supramolecular, Noncytotoxic, Stimuli-Responsive Hydrogels with Antibacterial Activity. *Biomacromolecules* **2017**, *18*, 3621−3629.

(20) Xu, X.; Zhang, D.; Gao, S.; Shiba, T.; Yuan, Q.; Cheng, K.; Tan, H.; Li, J. Multifunctional Biomaterial Coating Based on Bio-Inspired Polyphosphate and Lysozyme Supramolecular Nanofilm. *Biomacromolecules* **2018**, *19*, 1979−1989.

(21) Chandrika, N. T.; Garneau-Tsodikova, S. Comprehensive review of chemical strategies for the preparation of new aminoglycosides and their biological activities. *Chem. Soc. Rev.* **2018**, *47*, 1189−1249.

(22) Zhu, Y.; Xu, C.; Zhang, N.; Ding, X.; Yu, B.; Xu, F.-J. Polycationic Synergistic Antibacterial Agents with Multiple Functional Components for Efficient Anti-Infective Therapy. *Adv. Funct. Mater.* **2018**, *28*, 1706709.

(23) Sanchez-Lopez, E.; Gomes, D.; Esteruelas, G.; Bonilla, L.; Lopez-Machado, A. L.; Galindo, R.; Cano, A.; Espina, M.; Ettcheto, M.; Camins, A.; Silva, A. M.; Durazzo, A.; Santini, A.; Garcia, M. L.; Souto, E. B. Metal-Based Nanoparticles as Antimicrobial Agents: An Overview. *Nanomaterials* **2020**, *10*, 292.

(24) Jin, H.; Yang, L.; Ahonen, M. J. R.; Schoenfisch, M. H. Nitric Oxide-Releasing Cyclodextrins. *J. Am. Chem. Soc.* **2018**, *140*, 14178−14184.

(25) Machelart, A.; Salzano, G.; Li, X.; Demars, A.; Debrie, A.-S.; Menendez-Miranda, M.; Pancani, E.; Jouny, S.; Hoffmann, E.; Deboosere, N.; Belhaouane, I.; Rouanet, C.; Simar, S.; Talahari, S.; Giannini, V.; Villemagne, B.; Flipo, M.; Brosch, R.; Nesslany, F.; Deprez, B.; Muraille, E.; Locht, C.; Baulard, A. R.; Willand, N.; Majlessi, L.; Gref, R.; Brodin, P. Intrinsic Antibacterial Activity of Nanoparticles Made of β-Cyclodextrins Potentiates Their Effect as Drug Nanocarriers against Tuberculosis. *ACS Nano* **2019**, *13*, 3992−4007.

(26) Suárez, D. F.; Consuegra, J.; Trajano, V. C.; Gontijo, S. M. L.; Guimarães, P. P. G.; Cortés, M. E.; Denadai, Á. L.; Sinisterra, R. D. Structural and thermodynamic characterization of doxycycline/beta-cyclodextrin supramolecular complex and its bacterial membrane interactions. *Colloids Surf., B* **2014**, *118*, 194−201.

(27) Xu, H.; Fang, Z.; Tian, W.; Wang, Y.; Ye, Q.; Zhang, L.; Cai, J. Green Fabrication of Amphiphilic Quaternized beta-Chitin Derivatives with Excellent Biocompatibility and Antibacterial Activities for Wound Healing. *Adv. Mater.* **2018**, *30*, 1801100.

(28) Liang, L.; Chen, Y.; Chen, X.-M.; Zhang, Y.; Liu, Y. Cyclodextrin/polyethylenimine-based supramolecular nanoparticles for loading and sustained release of ATP. *Chin. Chem. Lett.* **2018**, *29*, 989−991.

(29) Li, F.; Ye, Q.; Gao, Q.; Chen, H.; Shi, S.; Zhou, W.; Li, X.; Xia, C.; Li, J. Facile Fabrication of Self-Healable and Antibacterial Soy Protein Based Films with High Mechanical Strength. *ACS. Appl. Mater. Interfaces* **2019**, *11*, 16107−16116.

(30) Funao, H.; Nagai, S.; Sasaki, A.; Hoshikawa, T.; Tsuji, T.; Okada, Y.; Koyasu, S.; Toyama, Y.; Nakamura, M.; Aizawa, M.; Matsumoto, M.; Ishii, K. A novel hydroxyapatite film coated with ionic silver via inositol hexaphosphate chelation prevents implant-associated infection. *Sci. Rep.* **2016**, *6*, 23238.

(31) Cui, Y.; Zhao, Y.; Tian, Y.; Zhang, W.; Lu, X.; Jiang, X. The molecular mechanism of action of bactericidal gold nanoparticles on Escherichia coli. *Biomaterials* **2012**, *33*, 2327−2333.

(32) Shi, L.; Liu, X.; Wang, W.; Jiang, L.; Wang, S. A Self-Pumping Dressing for Draining Excessive Biofluid around Wounds. *Adv. Mater.* **2019**, *31*, 1804187.

(33) Lv, M.; Su, S.; He, Y.; Huang, Q.; Hu, W.; Li, D.; Fan, C.; Lee, S.-T. Long-Term Antimicrobial Effect of Silicon Nanowires Decorated with Silver Nanoparticles. *Adv. Mater.* **2010**, *22*, 5463−5467.

(34) Wang, R.; Shi, M.; Xu, F.; Qiu, Y.; Zhang, P.; Shen, K.; Zhao, Q.; Yu, J.; Zhang, Y. Graphdiyne-modified TiO_2 nanofibers with osteoinductive and enhanced photocatalytic antibacterial activities to prevent implant infection. *Nat. Commun.* **2020**, *11*, 4465.

(35) Petter, R. C.; Salek, J. S.; Sikorski, C. T.; Kumaravel, G.; Lin, F. T. Cooperative binding by aggregated mono-6-(alkylamino)-β-cyclodextrins. *J. Am. Chem. Soc.* **1990**, *112*, 3860−3868.

(36) Foroughi, M.; Azqhandi, M. H. A.; Kakhki, S. Bio-inspired, high, and fast adsorption of tetracycline from aqueous media using Fe_3O_4-g-CN@PEI-beta-CD nanocomposite: Modeling by response surface methodology (RSM), boosted regression tree (BRT), and

https://doi.org/10.1021/acs.biomac.1c01007
Biomacromolecules XXXX, XXX, XXX−XXX

general regression neural network (GRNN). *J. Hazard. Mater.* **2020**, *388*, 121769.
(37) Lee, J. H.; Kwak, S.-Y. Branched polyethylenimine-polyethylene glycol-*β*-cyclodextrin polymers for efficient removal of bisphenol A and copper from wastewater. *J. Appl. Polym. Sci.* **2020**, *137*, 48475.
(38) Xu, W.; Chen, Y.; Liu, Y. Directional Water Transfer Janus Nanofibrous Porous Membranes for Particulate Matter Filtration and Volatile Organic Compound Adsorption. *ACS. Appl. Mater. Interfaces* **2021**, *13*, 3109−3118.
(39) Li, D.; Takarada, W.; Ashizawa, M.; Yamamoto, T.; Matsumoto, H. Effect of hydrogen-deuterium exchange in amide linkages on properties of electrospun polyamide nanofibers. *Polymer* **2021**, *229*, 123994.
(40) Sun, X.; Bai, L.; Li, J.; Huang, L.; Sun, H.; Gao, X. Robust preparation of flexibly super-hydrophobic carbon fiber membrane by electrospinning for efficient oil-water separation in harsh environments. *Carbon* **2021**, *182*, 11−22.
(41) Wang, C.; Wu, S.; Jian, M.; Xie, J.; Xu, L.; Yang, X.; Zheng, Q.; Zhang, Y. Silk nanofibers as high efficient and lightweight air filter. *Nano Res.* **2016**, *9*, 2590−2597.
(42) Zhao, D.; Yang, N.; Wei, Y.; Jin, Q.; Wang, Y.; He, H.; Yang, Y.; Han, B.; Zhang, S.; Wang, D. Sequential drug release via chemical diffusion and physical barriers enabled by hollow multishelled structures. *Nat. Commun.* **2020**, *11*, 4450.
(43) Guo, M.; Zhou, G.; Liu, Z.; Liu, J.; Tang, J.; Xiao, Y.; Xu, W.; Liu, Y.; Chen, C. Direct site-specific treatment of skin cancer using doxorubicin-loaded nanofibrous membranes. *Sci. Bull.* **2018**, *63*, 92−100.
(44) Xing, J.; Zhang, G.; Jia, X.; Liu, D.; Wyman, I. Preparation of Multipurpose Polyvinylidene Fluoride Membranes via a Spray-Coating Strategy Using Waterborne Polymers. *ACS. Appl. Mater. Interfaces* **2021**, *13*, 4485−4498.

https://doi.org/10.1021/acs.biomac.1c01007
Biomacromolecules XXXX, XXX, XXX−XXX